AFRL-SR-AR-TR-04-

REPORT DOCUMENTATION PAGE

0492

Public reporting burden for this collection of information is estimated to average 1 hour per response, including the time for reviewing instructi
needed, and completing and reviewing this collection of information. Send comments regarding this burden estimate or any other as⟂ct of t
Department of Defense, Washington Headquarters Services, Directorate for Information Operations and Reports (0704-0188), 1215 Jefferso
should be aware that notwithstanding any other provision of law, no person shall be subject to any penalty for failing to comply with a collectio⟂. ⟂⟂⟂⟂⟂⟂⟂ ⟂ ⟂⟂⟂ ⟂⟂ ⟂⟂⟂⟂⟂ ⟂⟂⟂⟂⟂ ⟂⟂⟂⟂ ⟂⟂⟂⟂⟂ ⟂⟂⟂⟂⟂.
PLEASE DO NOT RETURN YOUR FORM TO THE ABOVE ADDRESS.

1. REPORT DATE (DD-MM-YYYY)	2. REPORT TYPE	3. DATES COVERED (From - To)
01 Sep 2004	Final performance report	01 Dec 2000 — 31 May 2004

4. TITLE AND SUBTITLE	5a. CONTRACT NUMBER
Infrared activity of atom-doped solid hydrogen	
	5b. GRANT NUMBER
	AFOSR F49620-01-1-0068
	5c. PROGRAM ELEMENT NUMBER

6. AUTHOR(S)	5d. PROJECT NUMBER
Hinde, Robert J.	
	5e. TASK NUMBER
	5f. WORK UNIT NUMBER

7. PERFORMING ORGANIZATION NAME(S) AND ADDRESS(ES)	8. PERFORMING ORGANIZATION REPORT NUMBER
The University of Tennessee Department of Chemistry Knoxville, TN 37996-1600	

9. SPONSORING / MONITORING AGENCY NAME(S) AND ADDRESS(ES)	10. SPONSOR/MONITOR'S ACRONYM(S)
Air Force Office of Scientific Research	AFOSR
4015 Wilson Blvd. Room 713 Arlington, VA 22203-1954	11. SPONSOR/MONITOR'S REPORT NUMBER(S)

12. DISTRIBUTION / AVAILABILITY STATEMENT
Approved for public release; distribution unlimited.

20040930 023

13. SUPPLEMENTARY NOTES

14. ABSTRACT
A theoretical framework was developed for predicting the line shape and integrated intensities of dopant-induced features in the infrared absorption spectrum of solid molecular hydrogen matrices containing S-state atomic impurities, such as alkali metal atoms or rare gas atoms. Path integral Monte Carlo simulations of Ar-doped, Kr-doped, and Xe-doped solid molecular hydrogen were performed in order to provide testable quantitative predictions of the line shapes of dopant-induced features in these systems' infrared absorption spectra. The interaction-induced dipole moment of the Ar-H2 van der Waals dimer was computed using ab initio quantum chemical methods in order to provide input for future calculations of the integrated intensity of Ar-induced absorption features in Ar-doped solid hydrogen matrices.

15. SUBJECT TERMS
solid hydrogen; infrared spectroscopy; propulsion; propellant; high energy density matter

16. SECURITY CLASSIFICATION OF:			17. LIMITATION OF ABSTRACT	18. NUMBER OF PAGES	19a. NAME OF RESPONSIBLE PERSON
			UU	21	Robert J. Hinde
a. REPORT U	b. ABSTRACT U	c. THIS PAGE U			19b. TELEPHONE NUMBER (include area code) 865-974-3141

Standard Form 298 (Rev. 8-98)
Prescribed by ANSI Std. Z39.18

FINAL PERFORMANCE REPORT

Infrared activity of atom-doped solid hydrogen

Robert J. Hinde
University of Tennessee

1. Project objectives and summary of accomplishments

Specific impulse (I_{sp}) is a standard performance metric for rocket propulsion systems, a metric that measures the momentum transferred to the rocket per unit weight of propellant consumed. For the current state-of-the-art liquid oxygen–liquid hydrogen propellant system, $I_{sp} = 389$ s [Sut86]. However, if the hydrogen propellant contains Al atoms at a mole fraction of 5%, the theoretical I_{sp} of this propellant system increases by 9% to 425 s; if the hydrogen propellant contains 5% B atoms, the theoretical I_{sp} jumps to 470 s, for an improvement of 21% [Car93]. These potentially dramatic increases in performance sparked considerable interest, within both the Air Force Research Laboratory and the Air Force's contractor community, in the development of techniques for synthesizing gram-scale quantities of atom-doped solid H_2 with dopant mole fractions near 5%.

To guide and evaluate these synthetic techniques, it is imperative that researchers have a method for measuring accurately the concentration of atomic dopants in solid H_2 matrices with thicknesses on the order of one to several millimeters. For atomic dopants with allowed electronic transitions in the visible and ultraviolet spectral regions, such as Al and B atoms, electronic spectroscopy can quickly disclose the presence or absence of a dopant. However, these allowed electronic transitions become optically thick in millimeter-thick H_2 solids with atomic dopant concentrations above roughly 0.5% [Faj93]; consequently, electronic spectroscopy cannot provide quantitative concentration information in the concentration range of interest.

Atom-doped solid H_2 matrices also absorb weakly in the infrared (IR) spectral region [Faj98]. These dopant-induced IR absorption features arise from nominally IR inactive $Q_1(0)$ pure vibrational transitions of individual H_2 molecules in the matrix, transitions that become IR active in the presence of dopants [Hin03]. Because these dopant-induced

1

features are inherently weak [Faj98], 1-mm thick samples of doped solid H_2 will remain optically thin (with transmittance values of 0.1 or higher) even at dopant concentrations approaching 5%. This makes these features attractive prospects for measuring dopant concentrations in thick H_2 solids.

The objective of the research documented in this final performance report was the development of methods for computing, from first principles, the integrated intensity of these dopant-induced $Q_1(0)$ vibrational transitions in solid H_2 matrices containing atomic substitutional impurities. Progress toward this goal was made on several fronts for the case in which the impurity is an S-state atom such as an alkali metal atom or a rare gas atom: (1) The mechanism by which S-state atomic impurities generate IR activity in the vibrational coordinate of nearby H_2 molecules was elucidated. (2) A theoretical framework was established for computing the line shapes and integrated intensities of dopant-induced $Q_1(0)$ features in solid H_2 matrices. (3) Path integral Monte Carlo simulations of rare-gas-doped solid H_2 were performed. Based on these simulations, testable quantitative predictions were made for the dopant-induced $Q_1(0)$ line shapes in solid H_2 matrices containing Ar, Kr, or Xe atoms. (4) Ab initio calculations for Ar–H_2 dimers were performed to provide input for future calculations of the intensity of Ar-induced $Q_1(0)$ features in Ar-doped solid H_2.

2. Atom-induced infrared absorption features in solid hydrogen

The central accomplishment during the performance period covered by this final report is the development of a theoretical framework for understanding and interpreting the pure vibrational H_2 $Q_1(0)$ features induced by S-state atomic substitional impurities in the infrared (IR) absorption spectra of solid hydrogen matrices. This theoretical framework includes: (1) an explanation of the mechanism by which atomic impurities generate $Q_1(0)$ IR activity in neighboring H_2 molecules, and (2) a method for relating the line shape of the dopant-induced $Q_1(0)$ feature to the vibrational dependence of the dopant–H_2 potential energy surface.

Before describing this theoretical framework, we first review some of the relevant properties of pure solid H_2 [Sil80, Van83]. In solid H_2, the rotational and vibrational motions of individual H_2 molecules are essentially unperturbed by the interactions between adjacent molecules; hence the rotational and vibrational quantum numbers j and v of each molecule remain good quantum numbers in solid H_2 [Sil80, Van83]. The theoretical framework summarized in this final performance report assumes that these quantum numbers also remain good in solid H_2 matrices that have been doped with atomic substitutional

2

impurities. This will be the case if the dopant–H$_2$ interaction is only weakly anisotropic and only weakly dependent on the H$_2$ vibrational quantum number.

The ground state of the solid hydrogen crystal is solid parahydrogen (pH$_2$), a hexagonal close packed lattice [Van62] with nearest-neighbor spacing of 3.79 Å [Sil80] in which each H$_2$ molecule has the rotational quantum number $j = 0$. The rotational degrees of freedom of these $j = 0$ H$_2$ molecules are described by the isotropic spherical harmonic $Y_{00}(\theta, \phi)$; the pH$_2$ crystal is thus composed of spherically symmetric objects with multipole moments that are identically zero, and is held together by dispersion forces. The H$_2$ molecules in the pH$_2$ crystal can therefore be treated as point particles, each with an embedded vibrational degree of freedom. The translational zero point motion of individual molecules in the solid H$_2$ matrix is rather large, so that the width of the first peak in the radial distribution function for solid H$_2$ is approximately 18% of the nearest-neighbor distance, even in the $T = 0$ K limit [Sil80].

A. The induction mechanism

Consider the Q$_1$(0) vibrational excitation $(v, j) = (1, 0) \leftarrow (0, 0)$ of a single H$_2$ molecule in solid pH$_2$. Upon excitation, this molecule induces pairwise transition dipole moments with each of its neighbors, as indicated schematically in Fig. 1(a); these transition moments arise from short-range overlap interactions between pH$_2$ molecules [McK74, McK89, Mey89]. The high symmetry of the pH$_2$ crystal causes these pairwise transition moment vectors to sum to zero, as is clear from Fig. 1(a). The Q$_1$(0) transition is therefore IR inactive in the pure solid.

However, if one of the pH$_2$ molecules in the solid is replaced with an atomic substitutional impurity, the lattice symmetry is broken in the vicinity of the dopant. This symmetry breaking may arise both from physical restructuring of the pH$_2$ crystal lattice in the vicinity of the impurity (structural symmetry breaking) and from the fact that the dopant–pH$_2$ interactions generate a Q$_1$(0) transition moment that differs from the one associated with pH$_2$–pH$_2$ pairs (electrical symmetry breaking). In either case, the net transition moment for Q$_1$(0) excitations localized on molecules neighboring the impurity is nonzero, as shown in Fig. 1(b), and the vibrational coordinates of these molecules are therefore IR active. Atomic impurities thus induce IR absorption activity in pH$_2$ molecules in the host matrix as a direct consequence of the intermolecular interactions between the impurities and the pH$_2$ molecules.

Because the overlap interactions that give rise to the Q$_1$(0) transition moment are short-ranged, the pH$_2$ molecules that are in direct contact with the atomic impurity are the only ones that contribute directly to the intensity of the Q$_1$(0) transition. This observation plays a key role in our analysis of the dopant-induced Q$_1$(0) feature below.

B. The vibrational Hamiltonian of atom-doped solid parahydrogen

Here we consider dopant-induced $Q_1(0)$ absorption features in a crystal that contains N pH_2 molecules and an S-state atomic impurity. The position vector $\mathbf{R}_0$ denotes the impurity's position and the vectors $\{\mathbf{R}_n : n = 1, 2, 3, \ldots, N\}$ denote the centers of mass of the H_2 molecules in the crystal.

Because the vibrational motion of the pH_2 molecules occurs on a much faster time scale than any of the system's other motions, we make the simplifying assumption that the H_2 vibrations can be adiabatically separated from the other coordinates; we will use v_k to denote the vibrational quantum number of the H_2 molecule at $\mathbf{R}_k$. The crystal is therefore described completely by the position vectors $\{\mathbf{R}_0, \mathbf{R}_1, \mathbf{R}_2, \ldots, \mathbf{R}_N\}$ and the list of vibrational quantum numbers $\{v_1, v_2, \ldots, v_N\}$.

If the H_2–H_2 and dopant–H_2 potentials do not depend on the H_2 vibrational coordinates, then the translational degrees of freedom $\{\mathbf{R}_0, \mathbf{R}_1, \mathbf{R}_2, \ldots, \mathbf{R}_N\}$ decouple from the H_2 vibrational coordinates. In this limiting case, the wavefunction of the doped pH_2 solid can be written as the product of a translational wavefunction $\Psi(\mathbf{Q})$, where $\mathbf{Q} = \{\mathbf{R}_0, \mathbf{R}_1, \mathbf{R}_2, \ldots, \mathbf{R}_n\}$, and a wavefunction Φ that describes the vibrational degrees of freedom of the N H_2 molecules. When the H_2–H_2 and dopant–H_2 potentials depend only weakly on the H_2 vibrational coordinates, this separation of translational and vibrational degrees of freedom remains a good approximation to the doped solid's true wavefunction. Henceforth, this approximation is assumed to be valid, and the translational wavefunction $\Psi(\mathbf{Q})$ is assumed to be independent of the list of vibrational quantum numbers $\{v_1, v_2, \ldots, v_N\}$.

The initial state $|i\rangle$ of the doped pH_2 crystal, before the IR absorption event occurs, is one in which each H_2 molecule in the system is in its vibrational ground state. After IR excitation, the crystal is in a final state $|f\rangle$ whose vibrational wavefunction Φ can be described within an excitonic formalism [Fre31] as a linear combination of localized excitations residing on individual H_2 molecules. These localized excitations are denoted $|n, v\rangle$, which represents a localized state in which the vibrational quantum number of pH_2 molecule n is $v_n = v$, while the vibrational quantum number of all other pH_2 molecules is zero.

For the dopant-induced $Q_1(0)$ excitation, the crystal's final vibrational wavefunction Φ can be written as a linear combination of the $v = 1$ manifold of localized excitations. Hence the final state $|f\rangle$ is

$$|f\rangle = \Psi(\mathbf{Q}) \times \sum_n C_n |n, v = 1\rangle . \tag{1}$$

4

The coefficients $\{C_n\}$ that define the crystal's final state following IR excitation can be obtained by diagonalizing the excitonic Hamiltonian matrix $\mathbf{H}$ describing the vibrational degrees of freedom of the collection of N pH$_2$ molecules.

The Hamiltonian operator $\hat{H}$ of the doped pH$_2$ crystal depends on the translational variables $\mathbf{Q}$ and the H$_2$ vibrational quantum numbers $\{v_1, v_2, \ldots, v_N\}$ through the vibrationally averaged potential energy surface $V(\mathbf{Q}; v_1, v_2, \ldots, v_N)$ for the solid. The matrix elements of this operator in the basis of localized vibrational excitations can be written

$$H_{n',n} = \left\langle n', v = 1 \left| \left[\int \hat{H}(\mathbf{Q}; v_1, v_2, \ldots, v_N) \left| \Psi(\mathbf{Q}) \right|^2 d\mathbf{Q} \right] \right| n, v = 1 \right\rangle \tag{2}$$

and are seen to contain integrals over the probability density function $\left| \Psi(\mathbf{Q}) \right|^2$ for the translational zero point motion of the doped solid.

The diagonal Hamiltonian matrix element $H_{n,n}$ is simply the energy of the localized excited state $|n, v = 1\rangle$ in which the H$_2$ vibrational excitation resides on molecule n. The off-diagonal elements $H_{n',n}$ are averages over $\left| \Psi(\mathbf{Q}) \right|^2$ of the terms in the potential energy surface $V(\mathbf{Q}; v_1, v_2, \ldots, v_N)$ which couple the vibrational coordinates of pH$_2$ molecules n and n'.

The eigenvectors of $\mathbf{H}$ describe the final states accessed in the IR absorption event, as indicated in Eq. (1). The coefficients $\{C_n\}$ that describe a particular final state $|f\rangle$ are the elements of a column eigenvector of $\mathbf{H}$. The absorption intensity for this final state is proportional to the square of the corresponding transition dipole moment integral, which for dopant-induced Q$_1$(0) excitations is

$$\langle i | \mathbf{M} | f \rangle = \sum_n C_n \int \mathbf{M}_n(\mathbf{Q}) \left| \Psi(\mathbf{Q}) \right|^2 d\mathbf{Q} . \tag{3}$$

In Eq. (3), $\mathbf{M}_n(\mathbf{Q})$ is the Q$_1$(0) transition moment associated with excitation from the initial state $|i\rangle$ to the localized final state $|n, v = 1\rangle$. This transition moment depends, through $\mathbf{Q}$, on the structure of the doped pH$_2$ crystal in the neighborhood of the dopant. Finally, the dopant-induced Q$_1$(0) IR absorption line shape for a doped pH$_2$ solid can be obtained by weighting each final state $|f\rangle$ by its absorption intensity $\langle i | \mathbf{M} | f \rangle^2$.

The integrals in Eqs. (2) and (3) can be evaluated using quantum many-body techniques such as diffusion quantum Monte Carlo (DQMC) and path integral Monte Carlo (PIMC) simulations [And75, And99, Cep96, Cha81, Suh91]. These techniques provide computationally efficient methods for treating the large-amplitude correlated motion of neighboring molecules in the doped pH$_2$ solid. An accurate treatment of this large-amplitude motion is important for a number of reasons. First, the transition dipole moments $\mathbf{M}$ in Eq. (3) are dominated by overlap interactions between the dopant and its pH$_2$

5

neighbors. These transition moments depend strongly on the dopant–pH$_2$ distance [Mey89] and become substantially more important when they are averaged over the underlying zero point motion [Hin00]. Second, as Fig. 1 indicates, the transition dipole that controls the intensity of the dopant-induced IR absorption features is a *vector* quantity that depends simultaneously on the positions of the pH$_2$ molecule undergoing excitation, its impurity neighbor, and its eleven pH$_2$ neighbors. A faithful accounting of the correlated motions of these thirteen molecules is thus critical for computation of the transition moment.

C. A tight-binding model for the vibrational Hamiltonian

A simplified model for the vibrational Hamiltonian matrix **H** of doped pH$_2$ solids can be developed by extending the tight-binding vibron Hamiltonian introduced to explain the IR and Raman line shapes of pH$_2$ solids containing $j = 1$ H$_2$ molecules as dopants [Fel95, Sea64, Van59]. In this tight-binding vibron Hamiltonian, the vibrational coordinates of nearest-neighbor (nn) pH$_2$ molecules are assumed to be coupled through the H$_2$–H$_2$ intermolecular potential; pH$_2$ molecules which are not nearest neighbors are assumed to be remain decoupled. Under the assumption of only nearest-neighbor coupling, the tight-binding vibron Hamiltonian operator can be written as [Fel95]

$$\hat{H} = \sum_k E_k |k, v = 1\rangle\langle k, v = 1| + \lambda \sum_{k,n=\text{nn}} |k, v = 1\rangle\langle n, v = 1| \tag{4}$$

where $|n, v = 1\rangle$ again represents the state of the crystal in which the vibrational excitation is localized on pH$_2$ molecule n. In this equation, E_k is the Q$_1$(0) transition energy for the localized vibrational excitation associated with pH$_2$ molecule k; this transition energy can be obtained from Eq. (2) by setting $n' = n = k$. Intermolecular interactions in the solid reduce E_k from its gas phase value of $E_k = 4161.1$ cm^{-1} to $E_k = 4152.2$ cm^{-1} [Van68]. The parameter λ in Eq. (4) represents the vibrational coupling between nearest-neighbor molecules. Analysis of the IR absorption spectrum of pairs of $j = 1$ H$_2$ molecules isolated in solid pH$_2$ [Zha98] indicates that the hopping parameter $\lambda = -0.225$ cm^{-1} for a nearest-neighbor pair of H$_2$ molecules.

In a doped pH$_2$ crystal, the Q$_1$(0) transition energy E_k for pH$_2$ molecules next to an impurity will differ slightly from that for pH$_2$ molecules distant from the impurity because of differences between the H$_2$ vibrational dependence of the H$_2$–H$_2$ and dopant–H$_2$ potentials. We account for this by introducing a parameter ΔE that quantifies the shift in the Q$_1$(0) transition energy for pH$_2$ molecules adjacent to the dopant. For these molecules, $E_k = 4152.2$ cm$^{-1} - \Delta E$; for all other pH$_2$ molecules, E_k remains at 4152.2 cm^{-1}. This leads to a one-parameter family of vibron Hamiltonians defined by the parameter ΔE.

The matrix elements expressed in Eq. (2) are then equivalent to matrix elements of Eq. (4) evaluated in in a basis set consisting of the localized vibrational excitations $|n, v = 1\rangle$. Diagonalizing this matrix and then weighting the eigenvalues by their respective absorption intensities ultimately yields the dopant-induced $Q_1(0)$ line shape as described in section B above.

Figure 2 shows the normalized line shapes for several values of ΔE, ranging from 0.25 cm^{-1} to 2 cm^{-1}; the calculations leading to the results shown in Fig. 2 are described in detail in [Hin03]. At low values of the detuning parameter ΔE, the dopant-induced $Q_1(0)$ absorption feature shows substantial IR intensity over the entire pH$_2$ vibron band ranging from $\tilde{\nu} = 4149.5$ cm^{-1} to $\tilde{\nu} = 4153.1$ cm^{-1}. As ΔE increases, the dopant-induced absorption feature shifts to the red and sharpens; for $\Delta E = 2$ cm^{-1} the feature's full width at half maximum is only 0.02 cm^{-1}. This evolution in the shape of the dopant-induced feature as the detuning parameter increases reflects a transition from a delocalized IR-active vibron at small ΔE to a strongly localized IR-active vibron at large ΔE. When ΔE is small, the IR-active pH$_2$ molecules adjacent to the dopant can readily share their excitation with neighboring pH$_2$ molecules; consequently, the vibrons that contribute to the IR absorption spectrum can be quite spatially delocalized. As ΔE increases, however, it becomes more and more difficult for a vibrational excitation localized in the dopant's first "solvation shell" to hop away from the dopant, and the vibrational coordinates of pH$_2$ molecules in this solvation shell, which are the only IR-active molecules in the solid, become effectively decoupled from the rest of the system.

3. Detuning parameters for rare-gas-doped solid hydrogen

If the detuning parameter ΔE for a particular atomic dopant is known, the vibron Hamiltonian defined by Eq. (4) allows us to predict the line shape of the dopant-induced $Q_1(0)$ absorption feature in pH$_2$ solids containing this atomic dopant. We have used PIMC simulations to estimate the ΔE values for Ar, Kr, and Xe dopants in order to provide line shape predictions for these dopants that can eventually be compared with experiment.

The ΔE value for molecule k in a rare-gas-doped pH$_2$ solid can be estimated as

$$\Delta E^{(k)} = \int \Delta V^{(k)}(\mathbf{Q}) |\Psi(\mathbf{Q})|^2 \, d\mathbf{Q} \tag{5}$$

where the quantity

$$\Delta V^{(k)}(\mathbf{Q}) = V(\mathbf{Q}; v_1 = 0, v_2 = 0, \ldots, v_{k-1} = 0, v_k = 0, v_{k+1} = 0, \ldots, v_N = 0)$$
$$- V(\mathbf{Q}; v_1 = 0, v_2 = 0, \ldots, v_{k-1} = 0, v_k = 1, v_{k+1} = 0, \ldots, v_N = 0) \tag{6}$$

is the negative of the change in the potential energy of the doped pH_2 solid when molecule k makes a transition from its $v = 0$ vibrational level to its $v = 1$ vibrational level. (Recall that ΔE is defined above to be a positive number if the $Q_1(0)$ transition of a H_2 molecule red shifts under the influence of a neighboring dopant.) In principle this function can be decomposed into contributions from H_2–H_2 and dopant–H_2 potentials; however, at the moment there are no accurate H_2–H_2 potentials that explicitly incorporate vibrational dependence of the individual H_2 molecules. Consequently, we approximate $\Delta V^{(k)}(\mathbf{Q})$ as follows. We first assume that the 8.9-cm^{-1} red shift of the H_2 $Q_1(0)$ transition in pure solid pH_2 can be partitioned among an individual molecule's 12 nearest neighbors in an additive fashion. If molecule k is in the first solvation shell of the rare gas dopant, it has 11 pH_2 neighbors and is therefore missing $(1/12) \times 8.9 = 0.74$ cm^{-1} of this red shift. Consequently we define

$$\Delta V^{(k)}(\mathbf{Q}) = V_{\text{dop}-\text{H2}}(\mathbf{R}_0, \mathbf{R}_k; v = 0) - V_{\text{dop}-\text{H2}}(\mathbf{R}_0, \mathbf{R}_k; v = 1) - 0.74 \text{ cm}^{-1} \qquad (7)$$

where $V_{\text{dop}-\text{H2}}(\mathbf{R}_0, \mathbf{R}_k; v)$ is the rovibrationally averaged dopant–pH_2 potential for a pH_2 molecule in vibrational level v. Recall that the vectors $\mathbf{R}_0$ and $\mathbf{R}_k$ specify the locations of the dopant and pH_2 molecule k, respectively.

The integral in Eq. (5) is computed for doped pH_2 solids at $T = 4$ K using discrete-time PIMC simulations [Cha81] that employ the primitive Trotter factorization of the Boltzmann factor $\exp(-\hat{H}/kT)$. We model the rare-gas-doped pH_2 solid as a collection of 179 pH_2 molecules and one dopant atom at a number density equal to that of pure solid pH_2 at $T = 4$ K; the particles are initially placed on a hexagonal close packed lattice containing six layers of 30 particles each [Che96]. We use periodic boundary conditions to eliminate surface effects. The potential energy of the doped solid is taken to be a pairwise additive sum of H_2–H_2 potentials [Sil78] and dopant–H_2 potentials [LeR87]. We assume that the pH_2 molecules obey Boltzmann statistics.

Figure 3 shows how the ΔE value for pH_2 molecules surrounding an Ar dopant atom depends on the Trotter number N_T. We see that ΔE converges to the value $\Delta E = 0.20$ cm^{-1} for Trotter numbers $N_T \geq 48$. For our production calculations, we use the Trotter number $N_T = 64$. Our final estimates of the ΔE values for Ar-, Kr-, and Xe-doped pH_2 are: $\Delta E = 0.20$ cm^{-1} for Ar dopants, $\Delta E = 0.85$ cm^{-1} for Kr dopants, and $\Delta E = 1.68$ cm^{-1} for Xe dopants. The statistical uncertainties in these estimates are roughly ± 0.02 cm^{-1}.

These detuning parameters, when interpreted in light of the results summarized in Fig. 2, indicate that Ar-doped solid pH_2 should exhibit a broad, symmetric, featureless dopant-induced $Q_1(0)$ spectrum spanning the entire pH_2 vibron band; this is in good

agreement with experimental observations [Hin02]. Kr-doped solid pH_2 should exhibit an asymmetrical dopant-induced $Q_1(0)$ feature with peak intensity near $\tilde{\nu} = 4150.5 \text{ cm}^{-1}$, while Xe-doped solid pH_2 should exhibit a fairly narrow dopant-induced $Q_1(0)$ feature near $\tilde{\nu} = 4149.75 \text{ cm}-1$, with a low-intensity tail to the blue.

From our PIMC simulations, we can extract probability distribution functions for the distance between the dopant atom and its nearest-neighbor pH_2 molecules. These are shown in Figure 4. Each panel in Fig. 4 also includes, for reference purposes, the nearest-neighbor distance distribution for pure solid pH_2 at $T = 4$ K; this is computed using PIMC methods as well.

4. Ab initio calculations of the Ar–H_2 dipole moment

The integrated intensities of dopant-induced $Q_1(0)$ IR absorption features in atom-doped solid pH_2 are determined by the transition dipole moment integral defined in Eq. (3). This integral in turn depends on the $Q_1(0)$ transition moment $\mathbf{M}_n(\mathbf{Q})$ associated with excitation from the initial state $|i\rangle$ to the localized final state $|n, v = 1\rangle$. If the dipole moment operator for the doped pH_2 solid can be written as a pairwise sum of interaction-induced dipoles (see Fig. 1), then

$$\mathbf{M}_n(\mathbf{Q}) = \sum_k \mathbf{m}^{(k,n)}(\mathbf{R}_k, \mathbf{R}_n) \tag{8}$$

where $\mathbf{m}^{(k,n)}$ is the dipole moment generated by interactions between particles k and n, and the sum in Eq. (8) is over only the twelve nearest neighbors of pH_2 molecule n.

If n is a pH_2 molecule and k is either another pH_2 molecule or an S-state atomic dopant, then k and n are both spherically symmetric particles. The dipole moment function $\mathbf{m}^{(k,n)}$ then depends only on the interparticle vector $\mathbf{R}_{k,n} = \mathbf{R}_n - \mathbf{R}_k$. Furthermore, in this case $\mathbf{m}^{(k,n)}$ must point along the interparticle vector $\mathbf{R}_{k,n}$, so that we have

$$\mathbf{m}^{(k,n)} = \hat{\mathbf{R}}_{k,n} m^{(k,n)}(R_{k,n}) \tag{9}$$

where $m^{(k,n)}(R_{k,n})$ is now a scalar function of the interparticle distance $R_{k,n}$. The dependence of this function on the vibrational coordinate of pH_2 molecule n contains the essential information needed to predict the integrated intensities of dopant-induced $Q_1(0)$ features in doped pH_2 solids.

In the case that k and n are both pH_2 molecules, the vibrational dependence of this function has been computed using ab initio quantum chemical methods [Mey89]. Similar calculations are needed for dopant–pH_2 dimers to enable evaluation of the transition dipole

9

moment matrix elements defined by Eq. (3). We have used ab initio quantum chemical techniques to compute the interaction-induced dipole moment M for the Ar–H_2 dimer. This dipole moment is the derivative[1] of the Ar–H_2 interaction potential V with respect to the magnitude of an externally applied homogeneous electric field F: $M = (\partial V/\partial F)_{F=0}$. The interaction potential V is computed using Gaussian [Gau03] at the CCSD(T) level of theory employing the standard counterpoise correction [Boy70].

Our frozen-core calculations employ standard aug-cc-pVTZ atom-centered basis sets that have been extended with an additional set of diffuse functions. These additional functions consist of one primitive Gaussian of each symmetry with an exponent one-third as large as the smallest exponent of that symmetry in the standard aug-cc-pVTZ basis sets. Midway between the Ar nucleus and the H_2 center of mass, we place a (3s3p2d) set of bond functions [Tao92] to improve the description of dispersion interactions. Only valence electrons are correlated in our ab initio calculations. Extensive tests show that core–valence correlation makes an insignificant contribution to the interaction-induced dipole moment of the Ar–H_2 dimer.

We describe the configuration of the Ar–H_2 dimer using Jacobi coordinates, in which R is the Ar–H_2 distance, r is the H–H bond length, and γ is the angle between the Ar–H_2 vector and the H–H bond. For specificity, we place the dimer in the (x, z) plane with the Ar atom at the origin and the H_2 center of mass on the positive z axis; when $0 < \gamma < \pi/2$, the H atom which is closer to Ar has a positive x coordinate.

The derivative $(\partial V/\partial F)_{F=0}$ is estimated from a finite-difference analysis of the interaction energies obtained when the dimer is perturbed by external fields of strength $F = \pm 0.001$ au. Such an analysis gives accurate dipole moments if the interaction energy can be expressed as a quadratic function of the external field strength for small values of F; tests show that this is indeed the case for field strengths less than or equal to 0.003 au. Hence the finite-difference analysis employed here should give reliable dipole moments.

For the configuration ($R = 6.856$ a_0, $r = 1.401$ a_0, $\gamma = 0$), we obtain a field-free frozen-core Ar–H_2 interaction energy of $V = -52.50$ cm^{-1}; this is in excellent agreement with the value of -52.56 cm^{-1} obtained from a frozen-core CCSD(T) calculation [Woo98] employing the aug-cc-pV5Z basis set for H and the d-aug-cc-pV5Z basis set for Ar. This demonstrates that bond functions can effectively compensate for inadequacies of atom-centered Gaussian basis sets in computing the binding energy of weakly bound dimers.

---

[1] In Gaussian 03 revision B.05, the orientation of an externally applied field $\mathbf{F}$ is defined so that when a molecule's permanent dipole moment vector $\mathbf{M}$ points in the same direction as $\mathbf{F}$, the field–dipole interaction *raises* the molecule's energy.

Furthermore, we find that the interaction-induced dipole moment M changes by less than 1% when our extended triple-zeta basis sets are replaced by either larger aug-cc-pVQZ basis sets or smaller aug-cc-pVTZ basis sets. This indicates that the basis sets used here are large enough to yield converged interaction-induced dipole moments at the CCSD(T) level of theory.

At a fixed Ar–H_2 distance R, the Cartesian components of the interaction-induced dipole moment can be written as [Mey86a]

$$M_x = \sum_{k=0}^{\infty} \sum_{j=1}^{\infty} C_{2j,k} P_{2j}^1(\cos\gamma)(r - r_0)^k \tag{10}$$

and

$$M_z = \sum_{k=0}^{\infty} \sum_{j=0}^{\infty} D_{2j,k} P_{2j}(\cos\gamma)(r - r_0)^k \tag{11}$$

where P_n is a Legendre polynomial, P_n^m is an associated Legendre polynomial, and r_0 is a reference H–H bond length which we choose to be 1.4 a_0 here. Figure 5 shows the angular dependence of M_x and M_z for Ar–H_2 at $R = 5$ a_0 and $r = 1.4$ a_0. The ab initio results are accurately reproduced by a fit that includes the $j = 1$ term in Eq. (10) and the $j = 0$ through $j = 2$ terms in Eq. (11). To determine the number of powers of $(r - r_0)$ that must be retained in Eqs. (10) and (11), we calculate M_x and M_z for Ar–H_2 as functions of r at $R = 5$ a_0 and three values of γ; our results are shown in Fig. 6. We see that for r values between $r = 0.9$ a_0 and 2.1 a_0, truncating these power series expansions at $(r - r_0)^2$ is adequate.

Figures 5 and 6 show that we can determine the coefficients of the leading terms in Eqs. (10) and (11) for a given R value by computing the Ar–H_2 dipole moment at nine configurations, specified by three choices for r and three choices for γ. Here we choose $r = 1.1$, 1.4, and 1.7 a_0 and $\gamma = 0$, $\pi/4$, and $\pi/2$. We calculate the interaction-induced Ar–H_2 dipole moment at these nine configurations for several R values between 5 a_0 and 10 a_0. At a fixed value of R, we then integrate Eqs. (10) and (11) over specific H_2 rovibrational wavefunctions to obtain rovibrationally averaged dipole moments and rotationally averaged transition dipole moments. In Fig. 7, we present the rovibrationally averaged Ar–H_2 dipole moment

$$\langle M \rangle_{00} = \langle v = 0, j = 0 | M_z | v = 0, j = 0 \rangle \tag{12}$$

and the Ar–H_2 $Q_1(0)$ $v = 1 \leftarrow 0$ transition dipole moment

$$\langle M \rangle_{01} = \langle v = 0, j = 0 | M_z | v = 1, j = 0 \rangle \,. \tag{13}$$

11

In Eq. (13), the relative phases of the H_2 $v = 0$ and $v = 1$ vibrational wavefunctions are chosen so that the integral $\langle v = 0, j = 0|r|v = 1, j = 0 \rangle > 0$.

The $\langle M \rangle_{00}$ and $\langle M \rangle_{01}$ functions can be fit reasonably well by an expression of the form

$$\langle M \rangle = D_7/R^7 - c_0 \exp(c_1 R + c_2 R^2)$$

using these parameters (all in atomic units):

$$
\begin{aligned}
\langle M \rangle_{00} &: \quad D_7 = 278, \; c_0 = 29.815, \; c_1 = -1.1693, \; c_2 = -0.0543 \\
\langle M \rangle_{01} &: \quad D_7 = 166, \; c_0 = 4.450, \; c_1 = -0.9479, \; c_2 = -0.0496
\end{aligned}
\tag{14}
$$

Our $\langle M \rangle_{00}$ curve for Ar–H_2 is in qualitative agreement with that presented in [Mey86b], where the vibrationally averaged Ar–H_2 dipole moment $\langle M \rangle_{00}$ was estimated by performing ab initio calculations for Ar–H_2 dimers with the H_2 fragment frozen at its $v = 0$ vibrationally averaged bond length. If we evaluate the rotationally averaged ($j = 0$) Ar–H_2 dipole moment at this H–H bond length using Eqs. (10) and (11) and our computed C and D coefficients, our results are roughly 10% larger than those presented in [Mey86b] for Ar–H_2 distances R between 5 and 6 a_0.

5. Publications

6. References

[And75] J. B. Anderson, J. Chem. Phys. **63**, 1499 (1975).

[And99] J. B. Anderson, Rev. Comput. Chem. **13**, 133 (1999).

[Boy70] S. F. Boys and F. Bernardi, Mol. Phys. **19**, 553 (1970).

[Car93] P. G. Carrick, USAF Technical Report PL-TR-93-3014 (1993).

[Cep96] D. M. Ceperley and L. Mitas, Adv. Chem. Phys. **93**, 1 (1996).

[Cha81] D. Chandler and P. G. Wolynes, J. Chem. Phys. **74**, 4078 (1981).

[Che96] E. Cheng and K. B. Whaley, J. Chem. Phys. **104**, 3155 (1996).

[Faj93] M. E. Fajardo, J. Chem. Phys. **98**, 110 (1993).

[Faj98] M. E. Fajardo and S. Tam, J. Chem. Phys. **108**, 4237 (1998).

[Fel95] J. L. Feldman, J. H. Eggert, J. De Kinder, R. J. Hemley, H.-k. Mao, and D. Schoemaker, Phys. Rev. Lett. **74**, 1379 (1995).

[Fre31] J. Frenkel, Phys. Rev. **37**, 1276 (1931).

[Gau03] Gaussian 03, Revision B.03, a suite of computer programs written by M. J. Frisch *et al.* (2003).

[Hin00] R. J. Hinde, Phys. Rev. B **61**, 11451 (2000).

[Hin02] R. J. Hinde, D. T. Anderson, S. Tam, and M. E. Fajardo, Chem. Phys. Lett. **356**, 355 (2002).

[Hin03] R. J. Hinde, J. Chem. Phys. **119**, 6 (2003).

[LeR87] R. J. Le Roy and J. M. Hutson, J. Chem. Phys. **86**, 837 (1987).

[McK74] A. R. W. McKellar and H. L. Welsh, Can. J. Phys. **52**, 1082 (1974).

[McK89] A. R. W. McKellar, J. Chem. Phys. **92**, 3261 (1989).

[Mey86a] W. Meyer and L. Frommhold, Phys. Rev. A **34**, 2771 (1986).

[Mey86b] W. Meyer and L. Frommhold, Phys. Rev. A **34**, 2936 (1986).

[Mey89] W. Meyer, A. Borysow, and L. Frommhold, Phys. Rev. A **40**, 6931 (1989).

[Sea64] V. F. Sears and J. Van Kranendonk, Can. J. Phys. **42**, 980 (1964).

[Sil78] I. F. Silvera and V. V. Goldman, J. Chem. Phys. **69**, 4209 (1978).

[Sil80] I. F. Silvera, Rev. Mod. Phys. **52**, 393 (1980).

[Suh91] M. A. Suhm and R. O. Watts, Phys. Rep. **204**, 293 (1991).

[Sut86] G. P. Sutton, *Rocket Propulsion Elements* (Wiley-Interscience, New York, 1986).

[Tao92] F.-M. Tao and Y. K. Pan, J. Chem. Phys. **97**, 4989 (1992).

[Van59] J. Van Kranendonk, Physica **25**, 1080 (1959).

[Van62] J. Van Kranendonk and H. P. Gush, Phys. Lett. **1**, 22 (1962).

[Van68] J. Van Kranendonk and G. Karl, Rev. Mod. Phys. **40**, 531 (1968).

[Van83] J. Van Kranendonk, *Solid Hydrogen* (Plenum, New York, 1983).

[Woo98] D. E. Woon, K. A. Peterson, and T. H. Dunning, Jr., J. Chem. Phys. **109**, 2233 (1998).

[Zha98] Y. Zhang, T. J. Byers, M.-C. Chan, T. Momose, K. E. Kerr, D. P. Weliky, and T. Oka, Phys. Rev. B **58**, 218 (1998).

Figure 1. Symmetry breaking induces IR activity in solid pH_2 matrices containing atomic substitutional impurities. Open single circles represent $v = 0$ pH_2 molecules; double circles represent pH_2 molecules undergoing a $v = 1 \leftarrow 0$ excitation. (a) In a close packed pure pH_2 solid, excitation of a single pH_2 molecule generates twelve transition dipole moment vectors, six of which are shown here. The twelve vectors sum to zero because of the underlying symmetry of the close packed lattice. (b) In a pH_2 solid containing an atomic substitutional impurity (shaded circle), excitation of a pH_2 molecule next to the impurity yields a nonzero net transition dipole moment because the transition moment for dopant–pH_2 dimers differs from that for pH_2–pH_2 dimers.
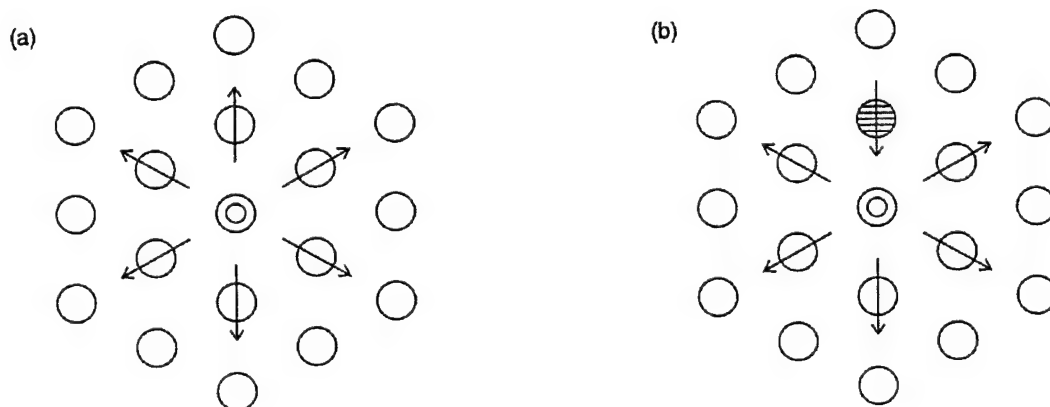
Figure 2. Theoretical dopant-induced pH_2 $Q_1(0)$ absorption spectra for several values of the detuning parameter ΔE. From bottom to top, $\Delta E = 0.25$ cm^{-1}, 0.5 cm^{-1}, 0.75 cm^{-1}, 1 cm^{-1}, 1.5 cm^{-1}, and 2 cm^{-1}. The spectra are offset vertically for clarity. Note that the spectra for $\Delta E \geq 1$ cm^{-1} have been reduced in intensity for ease of presentation.
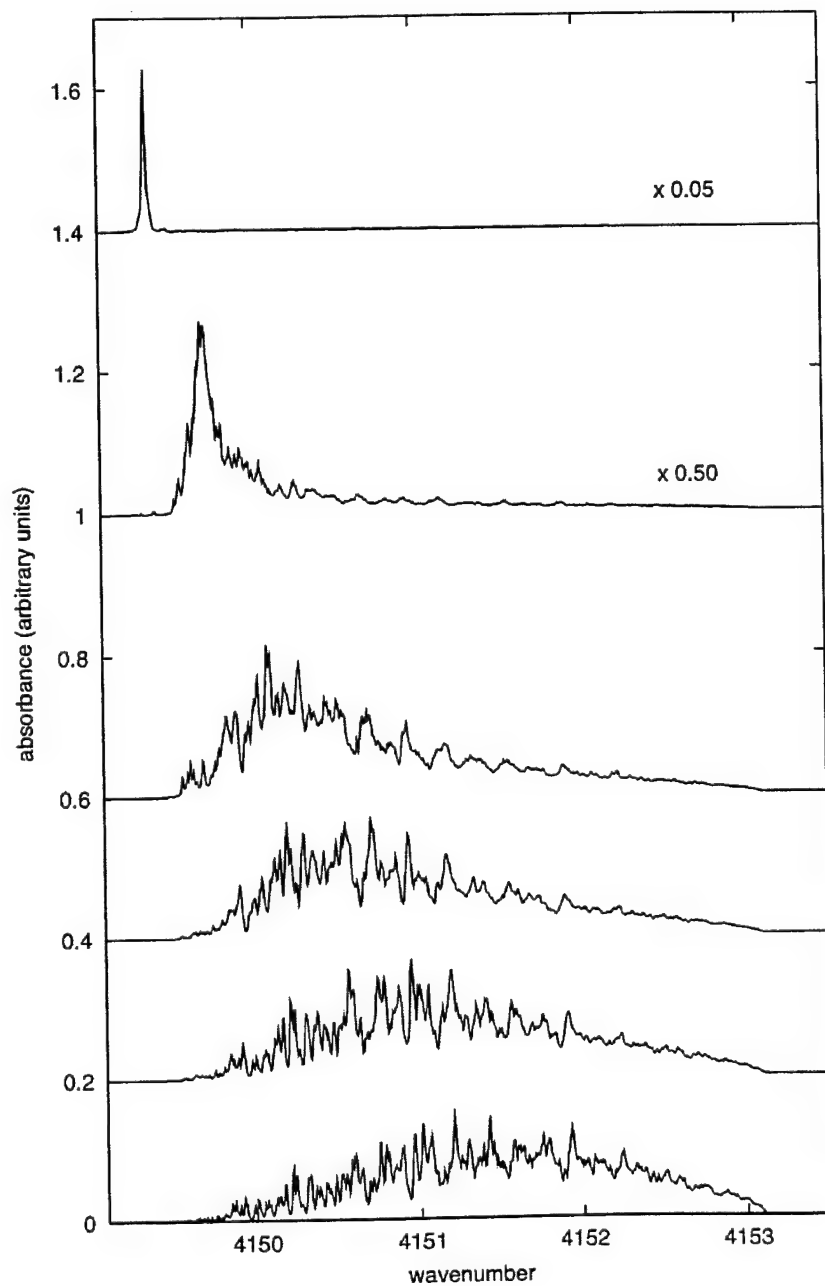
Figure 3. Convergence of ΔE for Ar-doped solid pH_2 with Trotter number N_T. For $N_T \geq 48$, ΔE converges to its asymptotic value of 0.20 cm^{-1}.
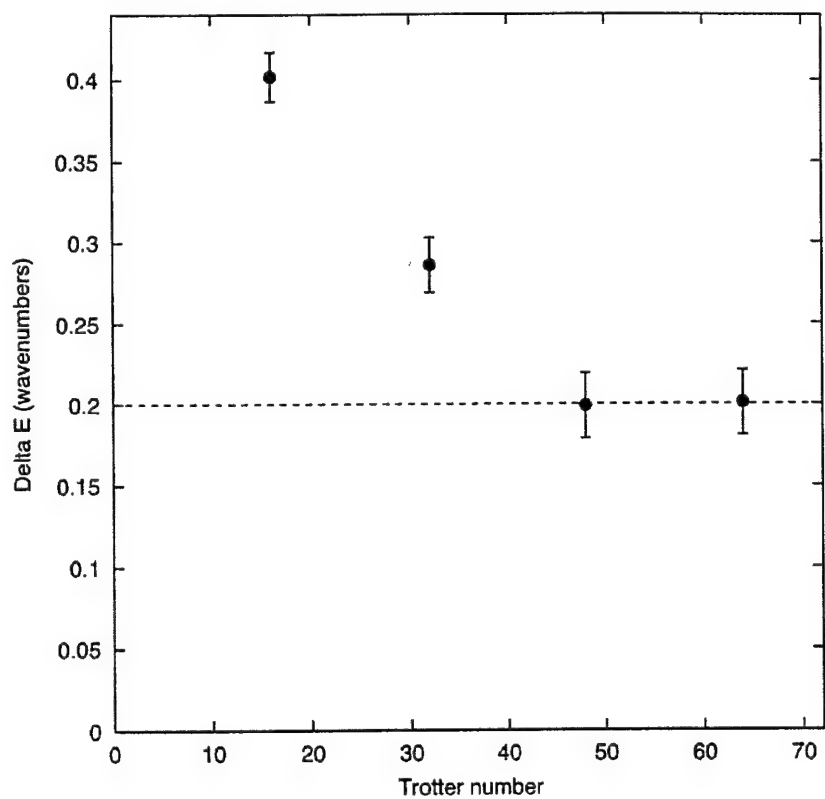
Figure 4. Distribution of dopant–H_2 nearest-neighbor distances in (a) Ar-doped, (b) Kr-doped, and (c) Xe-doped solid pH_2 at $T = 4$ K. The dashed line in each panel represents the distribution of nearest-neighbor H_2–H_2 distances in pure solid pH_2 at $T = 4$ K.
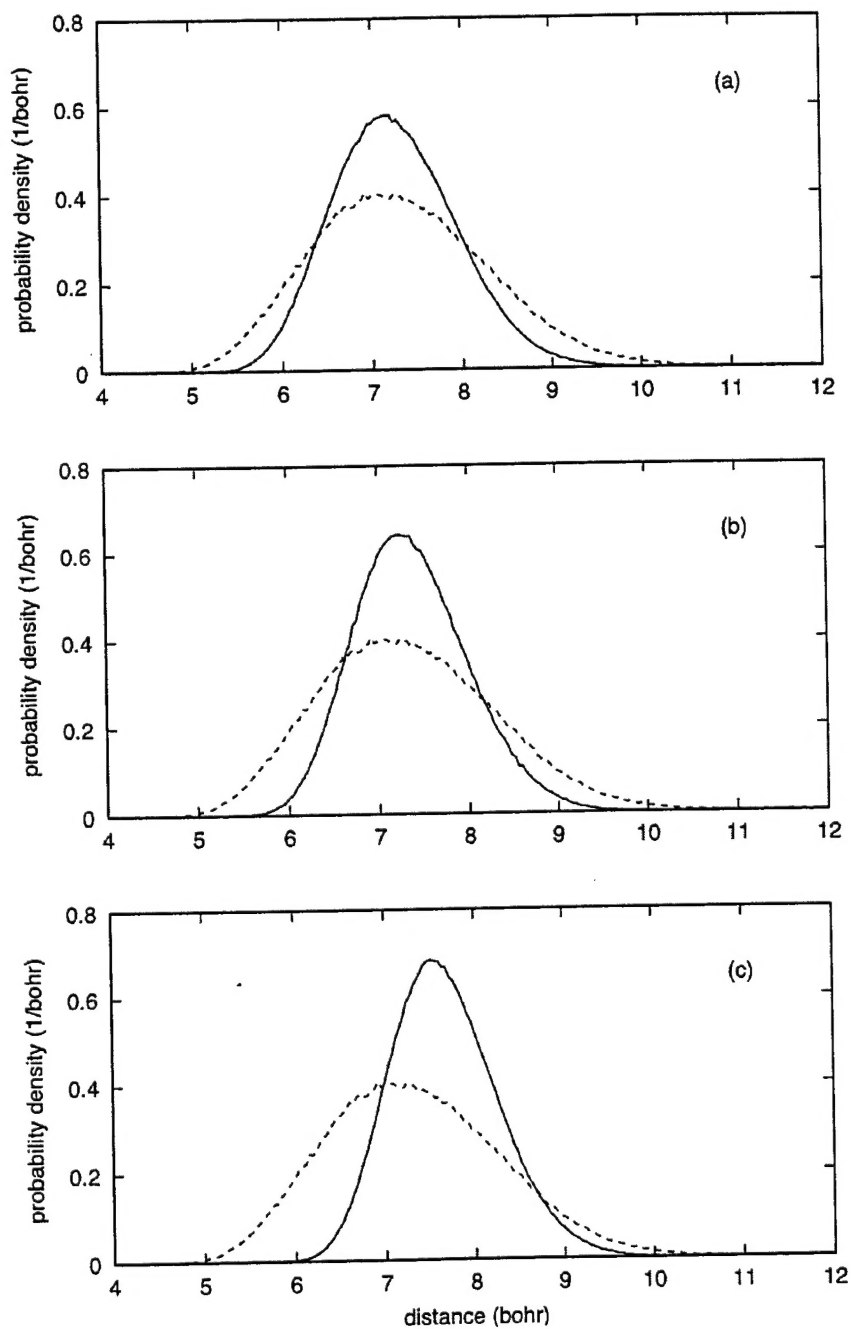
Figure 5. Dependence of the Ar–H$_2$ dipole moment on γ at $R = 5\ a_0$ and $r = 1.4\ a_0$. Open circles indicate values of M_x; open squares indicate values of M_z. The lines are fits to truncated Legendre polynomial expansions as described in the body of the report.
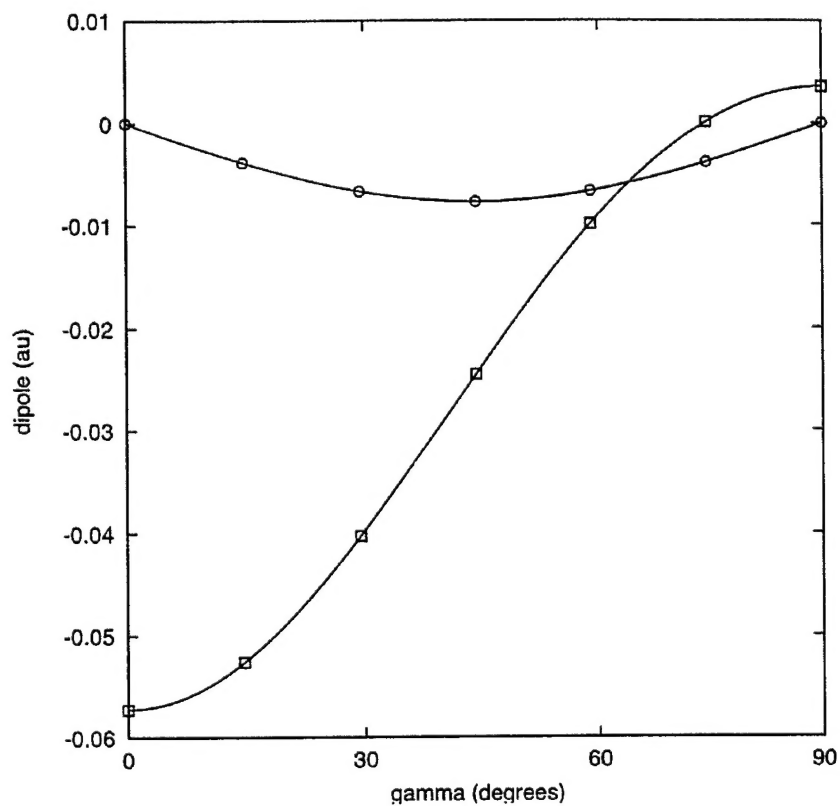
Figure 6. Dependence of the Ar–H$_2$ dipole moment on r at $R = 5\ a_0$. Panel (a) shows M_x as a function of r at $\gamma = \pi/4$; panel (b) shows M_z as a function of r at three γ values. The solid lines are quadratic fits to the ab initio calculations.
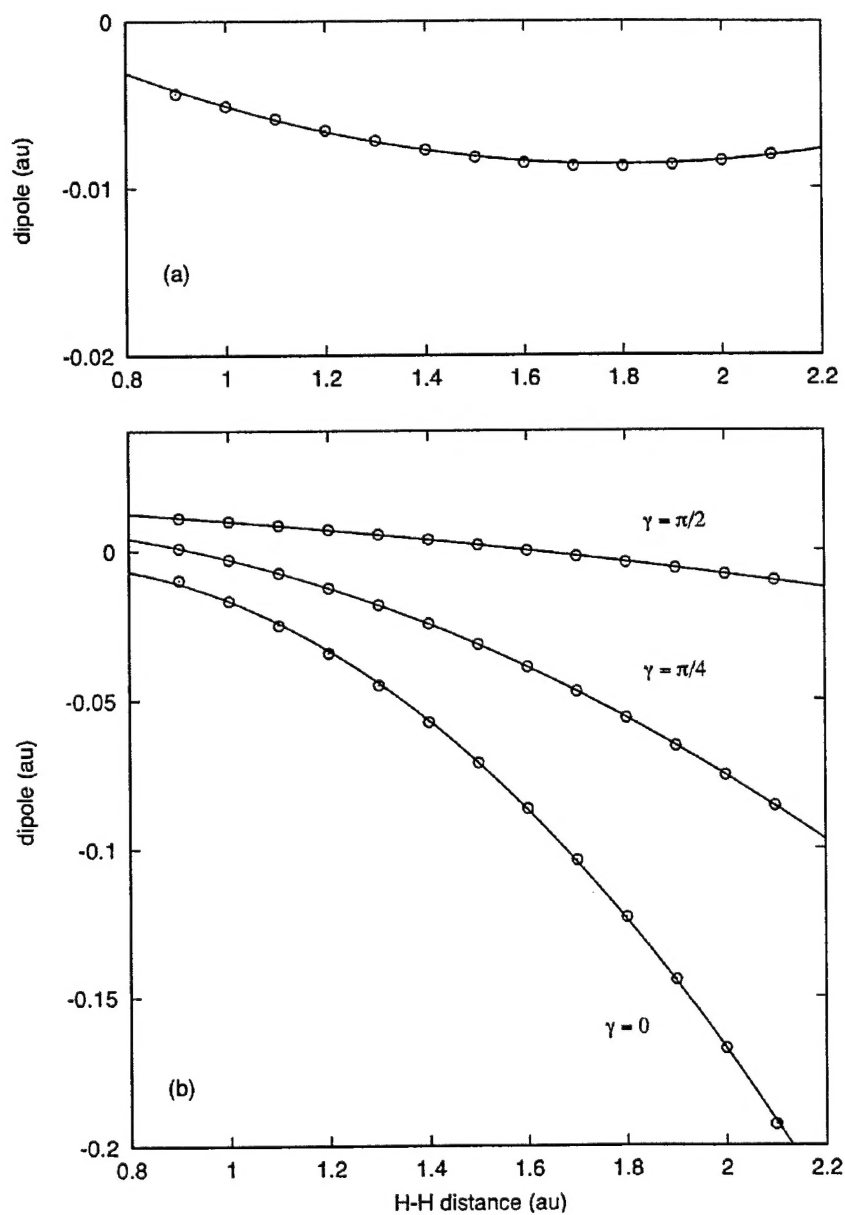
Figure 7. Dependence on R of (a) the rovibrationally averaged Ar–H$_2$ dipole moment $\langle M \rangle_{00}$ and (b) the Ar–H$_2$ $Q_1(0)$ transition dipole moment $\langle M \rangle_{01}$. The solid lines are cubic spline fits to the data. Note the change from linear to logarithmic scale in each plot at $\langle M \rangle = -2 \times 10^{-5}$ au.